Journal of *Marine Science and Engineering*

MDPI

Article

Formation Control of Unmanned Vessels with Saturation Constraint and Extended State Observation

Huixuan Fu, Shichuan Wang, Yan Ji and Yuchao Wang *

College of Intelligent Systems Science and Engineering, Harbin Engineering University, Harbin 150001, China; fuhuixuan@hrbeu.edu.cn (H.F.); wangshichuan@hrbeu.edu.cn (S.W.); jiyan@hrbeu.edu.cn (Y.J.)
* Correspondence: wangyuchao@hrbeu.edu.cn

Abstract: This paper addressed the formation control problem of surface unmanned vessels with model uncertainty, parameter perturbation, and unknown environmental disturbances. A formation control method based on the control force saturation constraint and the extended state observer (ESO) was proposed. Compared with the control methods which only consider the disturbances from external environment, the method proposed in this paper took model uncertainties, parameter perturbation, and external environment disturbances as the compound disturbances, and the ESO was used to estimate and compensate for the disturbances, which improved the anti-disturbance performance of the controller. The formation controller was designed with the virtual leader strategy, and backstepping technique was designed with saturation constraint (SC) function to avoid the lack of force of the actuator. The stability of the closed-loop system was analyzed with the Lyapunov method, and it was proved that the whole system is uniformly and ultimately bounded. The tracking error can converge to arbitrarily small by choosing reasonable controller parameters. The comparison and analysis of simulation experiments showed that the controller designed in this paper had strong anti-disturbance and anti-saturation performance to the compound disturbances of vessels and can effectively complete the formation control.

Keywords: formation control; extended state observer; saturation constraint; model uncertainty; backstepping; unmanned vessels

Citation: Fu, H.; Wang, S.; Ji, Y.; Wang, Y. Formation Control of Unmanned Vessels with Saturation Constraint and Extended State Observation. *J. Mar. Sci. Eng.* **2021**, *9*, 772. https://doi.org/10.3390/jmse9070772

Academic Editors: Alessandro Ridolfi and Md Jahir Rizvi

Received: 17 April 2021
Accepted: 13 July 2021
Published: 16 July 2021

1. Introduction

In recent years, with the continuous progress of science and technology, the formation control of autonomous unmanned systems (AUSs) has become a new topic in the field of control research [1]. In general, unmanned ground vehicles (UGVs) [2], autonomous underwater vehicles (AUVs) [3], mobile robots [4], and unmanned vessels [5] can be regarded as AUSs [6]. AUSs have a host of advantages, such as high reliability, high fault tolerance, completing complex tasks, and improving the efficiency of operations. In order to improve the efficiency of completing the task, the control of a single vessel can no longer meet the demand, and formation control of multiple vessels is often required to complete the task [7]. Compared with a single vessel, multi-vessel cooperation has the advantages of fault tolerance and strong adaptability. Formation control can be applied to rescue missions, exploration of natural resources, environmental monitoring, vessel replenishment, etc. [8]. Therefore, the research on formation control of unmanned vessels is of great application value.

The formation control problem is related to the design of stabilizing, path-following, and tracking controllers [9]. At present, several control methods have been proposed for trajectory tracking, such as model predictive control (MPC) [10], backstepping technique [11,12], and sliding mode control (SMC) [13,14]. In the field of formation, Skjetne et al. early proposed a robust nonlinear control method for the nonlinear formation control problem of vessels [15]. After that, several methods were proposed to solve the formation of the multiple vessels, including behavior-based [16], leader–follower [17,18], and virtual

leader structure [19,20]. Kim et al. adopted a dynamic model of an AUV with nonuniform current disturbances to develop a high-gain observer (HGO) for an estimation of the three-dimensional current velocities along AUV trajectories [21]. A novel fault tolerant leader–follower formation control scheme was designed for a group of underactuated autonomous surface vessels with partially known control input gain functions, where the line-of-sight (LOS) range and angle tracking errors are required to be constrained [22]. Yu et al. studied the practical time-varying formation tracking problem with multiple leaders using neural networks [23].

Considering the existence of model uncertainty, unknown parameters, and external environment disturbances in the vessel model, Wang [24], Peng [25], Shojaei [26], and Sun [14] have proposed some methods to estimate them. Moreover, Liu et al. proposed a nonlinear disturbance observer-based backstepping finite-time sliding mode control scheme for trajectory tracking of underwater vehicles subject to unknown system uncertainties and time-varying external disturbances [27]. Peng et al. adopted an extended state observer (ESO) to recover the unmeasured velocities as well as to estimate compound uncertainty induced by internal model uncertainty and external disturbance [28]. These schemes can improve the anti-disturbance performance of vessels.

However, the control input saturation constraint of vessel was not considered in the literature mentioned above. That is to say, the designed control forces and torques were assumed to be provided by the vessel's actuators. However, in actual engineering practice, the forces and torques provided by the actuator have output constraints, which may not satisfy the design requirement. If such situation occurs, it will not only affect the stability of the formation and fail to complete the assigned task, but also may cause collision between vessels. Therefore, it is necessary to design the vessel controller with saturation constraint. Wei et al. considered the trajectory tracking of a marine surface vessel in the presence of output constraint and uncertainties and adopted an asymmetric barrier Lyapunov function to cope with the output constraints [29]. The formation control problem of underactuated leaders with input constraint and a yawing motion on the water surface was studied in [30]. The input constraint trajectory tracking of a single underactuated surface vessel (USV) was studied in [31]. Shojaei designed a neural adaptive controller compensates unknown dynamics and external disturbances. Actuators' saturation nonlinearity is compensated by multilayer neural networks [32]. To overcome the difficulty of nondifferentiable input constraint, a smooth hyperbolic tangent function was employed to approximate the asymmetric saturation function [33]. A novel model-free robust bottom following controller for a flight-style AUV with saturated actuator dynamics was presented with theoretic and numerical analysis [34]. In [35], generalized saturation constraint (SC) function was adopted to prevent actuator saturation, and a neural network was used to compensate for uncertain nonlinearity.

Based on the analysis of the above literatures, this paper adopted the ESO to estimate the model uncertainty, internal parameter perturbations, and external environmental disturbances of unmanned surface vessels. Moreover, according to the literature analysis [30–35], the formation control problem of multi-unmanned surface vessels under actuator saturation constraint is further studied in this paper.

The contributions of this paper are summarized as follows: (1) The model uncertainty, parameter perturbation and external disturbances are estimated by ESO. Compared with the approximation strategy of neural network and HGO, the ESO has a simpler structure, high implementation efficiency, and can improve the anti-disturbance of the system. (2) With the formation control strategy of the virtual leader, the formation will not affect the navigation of other vessels due to the failure of the leader vessel. (3) The proposed anti-saturation controller will not cause insufficient force in the actuator, which is more in line with practical application.

The remainder of this paper is structured as follows. In Section 2, the mathematical model and formation control objectives of unmanned vessels are introduced. In Section 3, the ESO is designed, and the formation controller is designed by combining backstepping

and generalized SC function. Comparative simulation results are shown and analyzed in Section 4 to demonstrate the effectiveness, anti-disturbance and anti-saturation of the proposed formation controller based on SC function, ESO and the virtual leader strategy. Finally, the conclusions are shown in Section 5.

2. Problem Formulation

2.1. Mathematical Model of Surface Unmanned Vessels

Surface vessels generally ignore the three degrees of freedom (3-DOF) motions of heave, roll and pitch, and only consider the 3-DOF motions of surge, sway, and yaw [36].

In the body coordinate system, the kinematics and dynamics equations of the i-th $(i = 1, \cdots, n)$ unmanned vessel can be written as:

$$\dot{\boldsymbol{\eta}}_i = \boldsymbol{R}(\boldsymbol{\psi}_i)\boldsymbol{v}_i \tag{1}$$

$$\boldsymbol{M}_i\dot{\boldsymbol{v}}_i + \boldsymbol{C}_i(\boldsymbol{v}_i)\boldsymbol{v}_i + \boldsymbol{D}_i(\boldsymbol{v}_i)\boldsymbol{v}_i + \boldsymbol{\tau}_{gi} = \boldsymbol{\tau}_i + \boldsymbol{\tau}_{di} \tag{2}$$

where $\boldsymbol{\eta}_i = [x_i, y_i, \psi_i]^{\mathrm{T}}$ is the position and heading of the vessel in the north-east-down coordinate system; $\boldsymbol{v}_i = [u_i, v_i, r_i]^{\mathrm{T}}$ is the surge velocity, sway velocity and yaw angular velocity in the body coordinate system; $\boldsymbol{R}(\psi_i)$ is the rotation matrix from the body coordinate system to the north-east-down coordinate system, which satisfies $\boldsymbol{R}^{-1}(\psi_i) = \boldsymbol{R}^{\mathrm{T}}(\psi_i)$; $\boldsymbol{M}_i$ is the vessel inertia matrix, which satisfies $\boldsymbol{M}_i = \boldsymbol{M}_i^{\mathrm{T}}$; $\boldsymbol{C}_i(\boldsymbol{v}_i)$ is the Coriolis centripetal force matrix containing added mass; $\boldsymbol{D}_i(\boldsymbol{v}_i)$ is the damping parameter matrix; $\boldsymbol{\tau}_{gi} = [\boldsymbol{\tau}_{ugi}, \boldsymbol{\tau}_{vgi}, \boldsymbol{\tau}_{rgi}]^{\mathrm{T}}$ is model uncertainty and internal disturbances for vessels; $\boldsymbol{\tau}_i = [\boldsymbol{\tau}_{ui}, \boldsymbol{\tau}_{vi}, \boldsymbol{\tau}_{ri}]^{\mathrm{T}}$ is the force and torque output by the controller; $\boldsymbol{\tau}_{di} = [\boldsymbol{\tau}_{udi}, \boldsymbol{\tau}_{vdi}, \boldsymbol{\tau}_{rdi}]^{\mathrm{T}}$ is the time-varying disturbances of external wind, wave and current.

The specific expressions of $\boldsymbol{R}(\psi_i)$, $\boldsymbol{M}_i$, $\boldsymbol{C}_i(\boldsymbol{v}_i)$ and $\boldsymbol{D}_i(\boldsymbol{v}_i)$ are as follows:

$$\boldsymbol{R}(\psi_i) = \begin{bmatrix} \cos(\psi_i) & -\sin(\psi_i) & 0 \\ \sin(\psi_i) & \cos(\psi_i) & 0 \\ 0 & 0 & 1 \end{bmatrix}, \boldsymbol{M}_i = \begin{bmatrix} m_{11i} & 0 & 0 \\ 0 & m_{22i} & m_{23i} \\ 0 & m_{32i} & m_{33i} \end{bmatrix},$$

$$\boldsymbol{C}_i(\boldsymbol{v}_i) = \begin{bmatrix} 0 & 0 & -m_{22i}v_i \\ 0 & 0 & m_{11i}u_i \\ m_{22i}v_i & -m_{11i}u_i & 0 \end{bmatrix}, \boldsymbol{D}_i(\boldsymbol{v}_i) = \begin{bmatrix} d_{11i} & 0 & 0 \\ 0 & d_{22i} & d_{23i} \\ 0 & d_{32i} & d_{33i} \end{bmatrix}$$

where d_{11i}, d_{22i}, d_{23i}, d_{32i} and d_{33i} denote the hydrodynamic damping, m_{11i}, m_{22i}, m_{23i}, m_{32i} and m_{33i} denote the ship inertia, which includes added mass during surge, sway, and yaw. The dynamic model of an unmanned vessel with 3-DOF is shown in Figure 1.

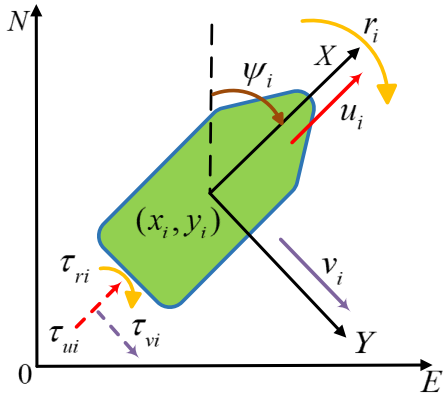

Figure 1. Dynamic model of an unmanned vessel with 3-DOF.

Figure 1 shows the 3-DOF motions of an unmanned vessel in the north-east-down coordinate system and the body coordinate system. N and E represent the north and east directions respectively in the north-east-down coordinate system.

In order to facilitate the design of the controller, Equation (1) is substituted into Equation (2) to obtain the mathematical model of the unmanned vessel in the north-east-down coordinate system, and it can be expressed as:

$$\bar{\boldsymbol{M}}_i(\boldsymbol{\eta}_i)\ddot{\boldsymbol{\eta}}_i + \bar{\boldsymbol{C}}_i(\boldsymbol{\eta}_i, \dot{\boldsymbol{\eta}}_i)\dot{\boldsymbol{\eta}}_i + \boldsymbol{\theta}_i(\boldsymbol{\eta}_i, \dot{\boldsymbol{\eta}}_i) = \boldsymbol{R}^{-\mathrm{T}}(\psi_i)\boldsymbol{\tau}_i \tag{3}$$

where

$$\dot{\boldsymbol{R}}(\psi_i) = \boldsymbol{R}(\psi_i) \cdot \begin{bmatrix} 0 & -r_i & 0 \\ -r_i & 0 & 0 \\ 0 & 0 & 0 \end{bmatrix},$$
$$\bar{\boldsymbol{M}}_i(\boldsymbol{\eta}_i) = \boldsymbol{R}^{-\mathrm{T}}(\psi_i)\boldsymbol{M}_i\boldsymbol{R}^{-1}(\psi_i),$$
$$\bar{\boldsymbol{C}}_i(\boldsymbol{\eta}_i, \dot{\boldsymbol{\eta}}_i) = -\boldsymbol{R}^{-\mathrm{T}}(\psi_i)\boldsymbol{M}_i\boldsymbol{R}^{-1}(\psi_i)\dot{\boldsymbol{R}}(\psi_i)\boldsymbol{R}^{-1}(\psi_i),$$
$$\boldsymbol{\theta}_i(\boldsymbol{\eta}_i, \dot{\boldsymbol{\eta}}_i) = \boldsymbol{R}^{-\mathrm{T}}(\psi_i)\boldsymbol{C}_i(\boldsymbol{v}_i)\boldsymbol{R}^{-1}(\psi_i)\dot{\boldsymbol{\eta}}_i + \boldsymbol{R}^{-\mathrm{T}}(\psi_i)\boldsymbol{D}_i(\boldsymbol{v}_i)\boldsymbol{R}^{-1}(\psi_i)\dot{\boldsymbol{\eta}}_i + \boldsymbol{R}^{-\mathrm{T}}(\psi_i)\boldsymbol{\tau}_{gi} - \boldsymbol{R}^{-\mathrm{T}}(\psi_i)\boldsymbol{\tau}_{di}$$

Notation 1. *In this paper, $|\cdot|$ stands for the absolute value of a scalar; $\|\cdot\|$ stands for the norm of the vector; $\hat{(\cdot)}$ stands for the estimate of $(\cdot)$;*

$\boldsymbol{\theta}_i(\boldsymbol{\eta}_i, \dot{\boldsymbol{\eta}}_i)$ is the compound disturbances composed of the unmodeled dynamics of the system, parameter perturbation and external disturbances. The converted model has the following properties:

(a) $\bar{\boldsymbol{M}}_i(\boldsymbol{\eta}_i)$ is a positive definite symmetric inertia matrix, and for $\forall \boldsymbol{x} \neq 0$, it satisfies $\lambda_{\min}(\bar{\boldsymbol{M}}_i(\boldsymbol{\eta}_i))\|\boldsymbol{x}\|_2^2 \leq \boldsymbol{x}^{\mathrm{T}}\bar{\boldsymbol{M}}_i(\boldsymbol{\eta}_i)\boldsymbol{x} \leq \lambda_{\max}(\bar{\boldsymbol{M}}_i(\boldsymbol{\eta}_i))\|\boldsymbol{x}\|_2^2$;

(b) $\dot{\bar{\boldsymbol{M}}}_i(\boldsymbol{\eta}_i) - 2\bar{\boldsymbol{C}}_i(\boldsymbol{\eta}_i, \dot{\boldsymbol{\eta}}_i)$ is obliquely symmetric, i.e., for any three-dimensional real number vector $\boldsymbol{\eta}_i$, it can get $\boldsymbol{\eta}_i^{\mathrm{T}}(\dot{\bar{\boldsymbol{M}}}_i(\boldsymbol{\eta}_i) - 2\bar{\boldsymbol{C}}_i(\boldsymbol{\eta}_i, \dot{\boldsymbol{\eta}}_i))\boldsymbol{\eta}_i = 0$;

(c) The damping matrix $\boldsymbol{D}_i(\boldsymbol{\eta}_i, \dot{\boldsymbol{\eta}}_i)$ is positive definite, and for $\forall \boldsymbol{\eta}_i \neq 0$, it satisfies $\boldsymbol{\eta}_i^{\mathrm{T}}\boldsymbol{D}_i(\boldsymbol{\eta}_i, \dot{\boldsymbol{\eta}}_i)\boldsymbol{\eta}_i > 0$;

(d) $\bar{\boldsymbol{C}}_i(\boldsymbol{\eta}_i, \boldsymbol{x}_1)\boldsymbol{x}_2 = \bar{\boldsymbol{C}}_i(\boldsymbol{\eta}_i, \boldsymbol{x}_2)\boldsymbol{x}_1$;

(e) $\bar{\boldsymbol{C}}_i(\boldsymbol{\eta}_i, \boldsymbol{x}_1 + \boldsymbol{x}_2)\boldsymbol{y} = \bar{\boldsymbol{C}}_i(\boldsymbol{\eta}_i, \boldsymbol{x}_1)\boldsymbol{y} + \bar{\boldsymbol{C}}_i(\boldsymbol{\eta}_i, \boldsymbol{x}_2)\boldsymbol{y}$;

(f) $\bar{\boldsymbol{C}}_i(\boldsymbol{\eta}_i, \boldsymbol{x}_1) \leq \lambda_{\mathrm{C}i}\|\boldsymbol{x}_1\|, \lambda_{\mathrm{C}i} \geq 0$.

2.2. Control Objective

First, the following assumptions are given:

Assumption 1. *The position information $\boldsymbol{\eta}_t(t)$ and velocity information $\boldsymbol{v}_t(t)$ of the virtual leader vessel can be obtained by each following vessel, and the position and velocity information of the following leader can also be measured by GPS. $\boldsymbol{\eta}_t(t)$ is a continuous differentiable function that changes with time t, and its first and second derivatives are bounded.*

Assumption 2. *Only the collaborative control of forward navigation of the leader is considered, i.e., the vessel's forward velocity $u > 0$.*

Assumption 3. *The internal unmodeled dynamics and the parameter perturbation compound function $\boldsymbol{\tau}_{gi}$ and the external environment disturbances $\boldsymbol{\tau}_{di}$ are both continuously bounded, and satisfy that $|\boldsymbol{\tau}_{gi}| \leq \boldsymbol{\tau}_{gi\mathrm{M}}$, $|\boldsymbol{\tau}_{di}| \leq \boldsymbol{\tau}_{di\mathrm{M}}$, where $\boldsymbol{\tau}_{gi\mathrm{M}}$ and $\boldsymbol{\tau}_{di\mathrm{M}}$ are unknown positive constants.*

According to the above assumptions, the desired trajectory of each follower vessel in the formation can be obtained by setting the position and heading angle error $\boldsymbol{\varepsilon}_i = [x_{\varepsilon i}, y_{\varepsilon i}, \psi_{\varepsilon i}]^{\mathrm{T}}$ between the virtual leader vessel and the follower vessels [37], as follows:

$$\boldsymbol{\eta}_{di}(t) = \boldsymbol{\eta}_t(t) + \boldsymbol{R}(\psi_t)\boldsymbol{\varepsilon}_i \tag{4}$$

where $\boldsymbol{\eta}_t(t) = [x_t(t), y_t(t), \psi_t(t)]^{\mathrm{T}}$ is the trajectory point of the virtual leader vessel, and $\psi_t(t) = \arctan(\dot{y}_t(t)/\dot{x}_t(t))$, $\boldsymbol{\eta}_{di}(t)$ is the desired trajectory point of the i-th follower vessel. The formation control figure of unmanned vessels is shown in Figure 2.

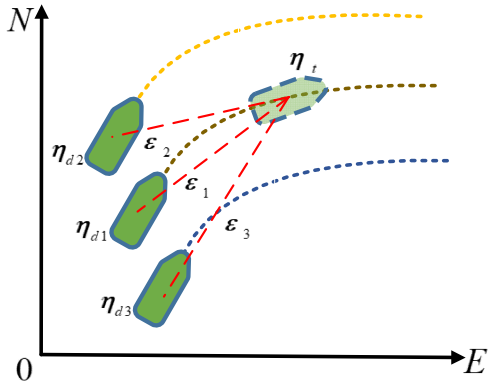

Figure 2. Formation control model of unmanned vessels.

Figure 2 shows the formation control of three unmanned vessels following the virtual leader vessel. It also shows the position error $\boldsymbol{\varepsilon}_i$ and the desired trajectory $\boldsymbol{\eta}_{di}(t)$. The control goal of this paper is to design $\boldsymbol{\tau}_i$ in Equation (2), and the generalized SC function and the nonlinear ESO are combined to obtain a formation controller with the ability of anti-saturation and anti-disturbance. The output saturation value of the force and torque by the actuator is considered. Then, the purpose of improving the control performance of the formation will be achieved. The controller makes all the signals in the closed-loop system consistent and ultimately bounded, and by selecting appropriate design parameters, the track and velocity tracking errors can be made arbitrarily small, i.e., satisfying:

$$\begin{aligned} \lim_{t\to\infty} \|\boldsymbol{\eta}_i(t) - \boldsymbol{\eta}_{di}(t)\| &\le \sigma_{1i} \\ \lim_{t\to\infty} \|\boldsymbol{v}_i(t) - \boldsymbol{v}_{di}(t)\| &\le \sigma_{2i} \end{aligned} \tag{5}$$

where $\boldsymbol{\eta}_i(t)$ is the actual track point of each vessel, $\boldsymbol{v}_{di}(t)$ and $\boldsymbol{v}_i(t)$ are the desired and the actual velocity vector of each vessel respectively, σ_{1i} and σ_{2i} are arbitrarily small positive constants. Equation (5) is the goal of coordinated control of multiple unmanned vessels, that is, through the decentralized coordinated control law, each unmanned vessel can achieve coordination in velocity and path, respectively.

3. Controller Design and Stability Analysis

The internal coupling, the parameter perturbation, and the disturbances of the external environmental disturbances are considered, the ESO is designed for feedback compensation to improve the anti-disturbance and control accuracy of the closed-loop system. In order to meet the engineering application, a generalized SC function with better performance is designed to solve the problem of actuator oversaturation and improve control performance. Then, according to the virtual leader formation strategy, combined with the backstepping control technique, the anti-disturbance and anti-saturation formation controller of the unmanned vessel is designed. Finally, the stability of the system is analyzed. The overall control structure of system is shown in Figure 3.

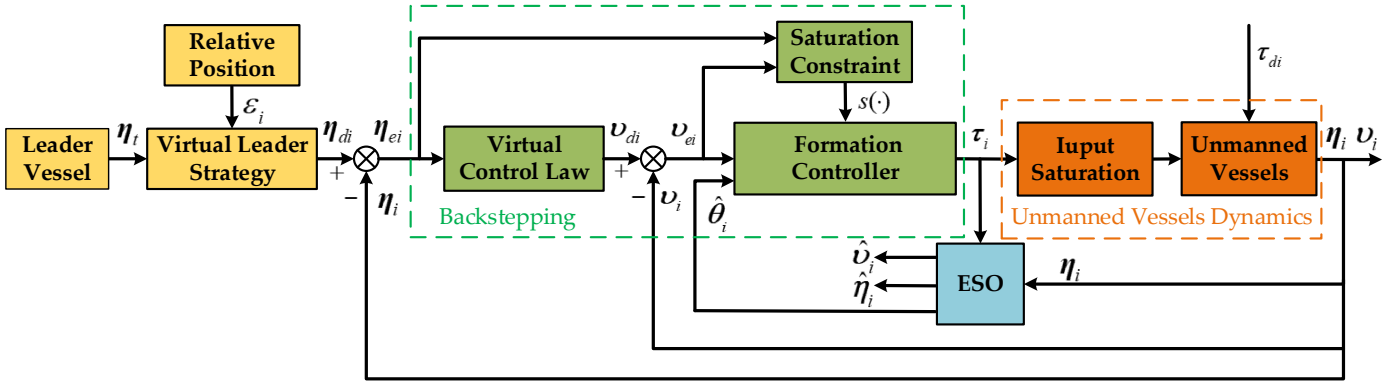

Figure 3. Control framework of the system.

As shown in Figure 3, the overall control structure of the system includes virtual leader strategy, backstepping technique, SC function, ESO, and unmanned vessel model.

3.1. Design of Extended State Observer

According to Equation (3), the dynamic model of the i-th unmanned vessel in the formation can be transformed into:

$$\ddot{\boldsymbol{\eta}}_i = \bar{\boldsymbol{M}}_i(\boldsymbol{\eta}_i)^{-1}(-\bar{\boldsymbol{C}}_i(\boldsymbol{\eta}_i, \dot{\boldsymbol{\eta}}_i)\dot{\boldsymbol{\eta}}_i) + \bar{\boldsymbol{M}}_i(\boldsymbol{\eta}_i)^{-1}(-\boldsymbol{\theta}_i(\boldsymbol{\eta}_i, \dot{\boldsymbol{\eta}}_i)) + \bar{\boldsymbol{M}}_i(\boldsymbol{\eta}_i)^{-1}\boldsymbol{R}^{-\mathrm{T}}(\psi_i)\boldsymbol{\tau}_i \tag{6}$$

To facilitate the design of the ESO, Equation (6) can be simplified as:

$$\ddot{\boldsymbol{\eta}}_i = \boldsymbol{G}_i + \boldsymbol{F}_i + \boldsymbol{B}_i\boldsymbol{u}_i \tag{7}$$

where $\boldsymbol{F}_i = \bar{\boldsymbol{M}}_i(\boldsymbol{\eta}_i)^{-2}(-\boldsymbol{\theta}_i(\boldsymbol{\eta}_i, \dot{\boldsymbol{\eta}}_i))$, $\boldsymbol{F}_i$ is the conversion form of compound disturbances; $\boldsymbol{B}_i = \boldsymbol{M}_i(\boldsymbol{\eta}_i)^{-1}\boldsymbol{R}^{-\mathrm{T}}(\psi_i)$, $\boldsymbol{G}_i = \bar{\boldsymbol{M}}_i(\boldsymbol{\eta}_i)^{-1}(-\bar{\boldsymbol{C}}_i(\boldsymbol{\eta}_i, \dot{\boldsymbol{\eta}}_i)\dot{\boldsymbol{\eta}}_i)$; $\boldsymbol{x}_{1i} = \boldsymbol{\eta}_i$ and $\boldsymbol{x}_{2i} = \dot{\boldsymbol{\eta}}_i$ are the state variable of the system; the control input $\boldsymbol{u}_i = \boldsymbol{\tau}_i$.

Then, the second-order system of each vessel in the formation can be expressed as:

$$\begin{cases} \dot{\boldsymbol{x}}_{1i} = \boldsymbol{x}_{2i} \\ \dot{\boldsymbol{x}}_{2i} = \boldsymbol{G}_i + \boldsymbol{F}_i + \boldsymbol{B}_i\boldsymbol{u}_i \\ \boldsymbol{y}_i = \boldsymbol{x}_{1i} \end{cases} \tag{8}$$

where $\boldsymbol{x}_{3i} = \boldsymbol{F}_i$ is the expansion state of the system, $\boldsymbol{y}_i$ is the system output. Assuming that the unknown compound disturbances $\boldsymbol{F}_i$ is smooth and bounded, and its first derivative satisfies $\sup\left\{\|\ell_i\| = \|\dot{\boldsymbol{F}}_i\|\right\} \leq \xi, \exists\xi > 0$, then, the following third order ESO is designed:

$$\begin{cases} \boldsymbol{e}_{1i} = \boldsymbol{z}_{1i} - \boldsymbol{x}_{1i} = \boldsymbol{z}_{1i} - \boldsymbol{\eta}_i \\ \dot{\boldsymbol{z}}_{1i} = \boldsymbol{z}_{2i} - \lambda_1 \mathrm{fal}(\boldsymbol{e}_{1i}, \beta, \delta_1) \\ \dot{\boldsymbol{z}}_{2i} = \boldsymbol{z}_{3i} + \boldsymbol{G}_i + \boldsymbol{B}_i\boldsymbol{u}_i - \lambda_2 \mathrm{fal}(\boldsymbol{e}_{1i}, \beta, \delta_2) \\ \dot{\boldsymbol{z}}_{3i} = -\lambda_3 \mathrm{fal}(\boldsymbol{e}_{1i}, \beta, \delta_3) \end{cases} \tag{9}$$

where $\boldsymbol{z}_{1i}$ and $\boldsymbol{z}_{2i}$ observe $\boldsymbol{\eta}_i$ and $\dot{\boldsymbol{\eta}}_i$ respectively, $\boldsymbol{z}_{3i}$ is the estimated value of $\boldsymbol{F}_i$, $\mathrm{fal}(\omega, \beta, \delta) = \begin{cases} |\omega|^{\beta}\mathrm{sgn}(\omega), |\omega| > \delta \\ \frac{\omega}{\delta^{1-\beta}}, |\omega| \leq \delta \end{cases}$, ω is the variable of the fal function, δ is an arbitrarily small positive number, $\beta \in (0, 1)$, λ_1, λ_2 and λ_3 are the observer parameters.

There is a coupling relationship among the 3-DOF motions of surge, sway, and yaw of the vessel. In active disturbance rejection control, the coupling within the model can be regarded as internal disturbances, and vessel parameter perturbation is usually also regarded as internal disturbances, i.e., model uncertainty. The external environment dis-

turbances are the external disturbances. When using the ESO to estimate, the internal and external disturbances are not distinguished, and they are regarded as a kind of compound disturbances.

Therefore, the observation error of ESO is $\boldsymbol{e}_i = [\boldsymbol{e}_{1i}, \boldsymbol{e}_{2i}, \boldsymbol{e}_{3i}]^{\mathrm{T}}$, where $\boldsymbol{e}_{1i} = \boldsymbol{z}_{1i} - \boldsymbol{x}_{1i}$, $\boldsymbol{e}_{2i} = \boldsymbol{z}_{2i} - \boldsymbol{x}_{2i}$, $\boldsymbol{e}_{3i} = \boldsymbol{z}_{3i} - \boldsymbol{x}_{3i}$. According to Equation (8) and ESO (9), the error system equations of the observer can be obtained:

$$\begin{cases} \dot{\boldsymbol{e}}_{1i} = \boldsymbol{e}_{2i} - \lambda_1 \mathrm{fal}(\boldsymbol{e}_{1i}, \beta, \delta_1) \\ \dot{\boldsymbol{e}}_{2i} = \boldsymbol{e}_{3i} - \lambda_2 \mathrm{fal}(\boldsymbol{e}_{1i}, \beta, \delta_2) \\ \dot{\boldsymbol{e}}_{3i} = \ell_i - \lambda_3 \mathrm{fal}(\boldsymbol{e}_{1i}, \beta, \delta_3) \end{cases} \tag{10}$$

The following proves the convergence of the error system (10).

Proof. First, let $\boldsymbol{f}_i = \boldsymbol{e}_{1i}; \boldsymbol{f}_{1i} = \mathrm{fal}(\boldsymbol{e}_{1i}, \beta, \delta_1); \boldsymbol{f}_{2i} = \mathrm{fal}(\boldsymbol{e}_{1i}, \beta, \delta_2); \boldsymbol{g}_1(0) = 0, \boldsymbol{g}_1 = \mathrm{fal}(\boldsymbol{e}_{1i}, \beta, \delta_3)$, the following equations can be obtained:

$$\begin{cases} \boldsymbol{h}_2 = \boldsymbol{e}_{2i} - \lambda_1 \boldsymbol{f}_i + \mathrm{k}_1 \boldsymbol{g}_1 \mathrm{sgn}(\boldsymbol{e}_{1i}) \\ \boldsymbol{h}_3 = \boldsymbol{e}_{3i} - \lambda_2 \boldsymbol{f}_{1i} - \lambda_1 (\boldsymbol{e}_{2i} - \lambda_1 \boldsymbol{f}_i) + \mathrm{k}_2 \boldsymbol{g}_2 \mathrm{sat}(\boldsymbol{h}_2 / \boldsymbol{g}_1) \end{cases} \tag{11}$$

where $\mathrm{k}_1 > 1$ and $\mathrm{k}_2 > 1$; $\boldsymbol{g}_2$ is a continuous positive definite function, its expression is $\boldsymbol{g}_2 = \begin{cases} \mathrm{k}_3 |\boldsymbol{h}_2|, |\boldsymbol{h}_2| \geq \boldsymbol{g}_1 \\ \mathrm{k}_3 |\boldsymbol{g}_1|, |\boldsymbol{h}_2| < \boldsymbol{g}_1 \end{cases}$; the constant $\mathrm{k}_3 > \frac{(\mathrm{k}_1+1)^2}{(\mathrm{k}_2-1)^2} \left| \frac{\mathrm{d}\boldsymbol{g}_1}{\mathrm{d}\boldsymbol{g}_2} \right|, \boldsymbol{g}_2(0,0) = 0$.

Lemma 1. *If the parameters λ_1, λ_2 and λ_3 in the extended state observer (9) meet the following conditions* [38]

$\lambda_1 - \mathrm{k}_2\mathrm{k}_3 > \left| \frac{\lambda_2 \boldsymbol{f}'_{1i}}{\mathrm{k}_3} - \lambda_1\mathrm{k}_2 - \mathrm{k}_1\mathrm{k}_2 \frac{\mathrm{d}\boldsymbol{g}_1 \boldsymbol{s}}{\mathrm{d}\boldsymbol{e}_{1i}} + \mathrm{k}_2^2\mathrm{k}_3 \right| + \max\left\{ \mathrm{k}_3 + \left| \mathrm{k}_1 \frac{\mathrm{d}\boldsymbol{g}_1 \boldsymbol{s}}{\mathrm{d}\boldsymbol{e}_{1i}} - \mathrm{k}_2\mathrm{k}_3 \right| + \mathrm{k}_1^2 \left| \frac{\mathrm{d}\boldsymbol{g}_1 \boldsymbol{s}}{\mathrm{d}\boldsymbol{e}_{1i}} \right|, (1+\mathrm{k}_1) \frac{\mathrm{d}\boldsymbol{g}_1 \boldsymbol{s}}{\mathrm{d}\boldsymbol{e}_{1i}} \right\}$
$+ \frac{1}{\mathrm{k}_3} \left| \lambda_3 \frac{|\boldsymbol{f}_{2i}|}{\boldsymbol{g}_1} - \lambda_2 \mathrm{k}_1 \boldsymbol{f}'_{2i} + \mathrm{k}_1\mathrm{k}_2\mathrm{k}_3 \frac{\mathrm{d}\boldsymbol{g}_1 \boldsymbol{s}}{\mathrm{d}\boldsymbol{e}_{1i}} \right|$, *where* $\boldsymbol{g}_1 \boldsymbol{s} = \boldsymbol{g}_1 \mathrm{sgn}(\boldsymbol{e}_{1i})$, $|\boldsymbol{f}_{2i}| = \boldsymbol{f}_{2i} \mathrm{sgn}(\boldsymbol{e}_{1i})$ *and* $\boldsymbol{f}'_{1i} = \frac{\mathrm{d}\boldsymbol{f}_{1i}}{\mathrm{d}\boldsymbol{e}_{1i}}$. *Then the error system (10) satisfies* $\lim_{t \to \infty} \|\boldsymbol{e}_i\| < \sigma$, *where σ is an arbitrarily small positive constant.*

Therefore, reasonable selection of parameters λ_1, λ_2 and λ_3 are required to meet the conditions in Lemma 1, and the ESO can estimate the actual value very well, i.e., $\boldsymbol{z}_{1i} \to \boldsymbol{x}_{1i}$, $\boldsymbol{z}_{2i} \to \boldsymbol{x}_{2i}$ and $\boldsymbol{z}_{3i} \to \boldsymbol{x}_{3i}$. It can be seen that the observation error of ESO converges to arbitrarily small. The proof is complete. □

According to the Equations (1)–(3) and ESO (9), it can be obtained: $\hat{\boldsymbol{\eta}}_i = \boldsymbol{z}_{1i}$, $\hat{\boldsymbol{v}}_i = \boldsymbol{R}^{-1}(\psi_i) \boldsymbol{z}_{2i}$, $\hat{\boldsymbol{\theta}}_i(\boldsymbol{\eta}_i, \dot{\boldsymbol{\eta}}_i) = \boldsymbol{M}_i(\boldsymbol{\eta}_i)^2 \boldsymbol{z}_{3i}$, $\hat{\boldsymbol{\eta}}_i$ and $\hat{\boldsymbol{v}}_i$ are the observed values of $\boldsymbol{\eta}_i$ and $\boldsymbol{v}_i$, respectively, $\hat{\boldsymbol{\theta}}_i(\boldsymbol{\eta}_i, \dot{\boldsymbol{\eta}}_i)$ is the estimated value of compound disturbances $\boldsymbol{\theta}_i(\boldsymbol{\eta}_i, \dot{\boldsymbol{\eta}}_i)$.

3.2. Formation Controller Design

Considering the saturation of the actuator, the generalized SC function of the controller can be designed.

Definition 1. [39] *Given a non-decreasing function and a positive number, the function satisfies the following conditions: (1) the function is a generalized saturation function (SC) of local Lipschitz; (2) $xs(x) > 0, \forall x \neq 0$; (3) $|s(x)| \leq \rho$, where x is arbitrary real number.*

Lemma 2. [39] *The generalized SC function $s : x \to s(x)$ is a strictly increasing continuous derivable function and it is bounded by ρ. There is a function $s' : x \to \mathrm{d}s(x)/\mathrm{d}x$ and a parameter $\gamma_1 > 0$. The generalized SC function satisfies the following properties:*

(1) $s'(x) > 0$ is bounded, $s'_{\mathrm{M}} \in (0, \infty)$ makes $0 < s'(x) < s'_{\mathrm{M}}$, where x is an arbitrary real number;

(2) When x is arbitrary real number, it satisfies: $s^2(\gamma_1 x)/(2\gamma_1 s'_{\mathrm{M}}) \leq \int_0^x s(\gamma_1 \varsigma)d\varsigma \leq \gamma_1 s'_{\mathrm{M}} x^2/2$;

(3) $\int_0^x s(\gamma_1 \varsigma)d\varsigma > 0, \forall x \neq 0$;

(4) When $x \to \infty$, *there is* $\int_0^x s(\gamma_1 \varsigma)d\varsigma \to \infty$;

(5) $|s(\gamma_1 x)| \leq s'_{\mathrm{M}}\gamma_1|x|$, *where* x is arbitrary real number;

(6) When $\gamma_1 \geq 1$, *there is* $s^2(x) \leq s^2(\gamma_1 x)$, *where* x *is arbitrary real number.*

According to the Definition 1 and Lemma 2, the following generalized SC function can be designed as:

$$s(e_j) = \begin{cases} -\omega_j + \dfrac{e_j+\omega_j}{\sqrt{1+(\frac{e_j+\omega_j}{\rho_j-\omega_j})^2}}, & \forall e_j < -\omega_j \\ e_j, & \forall e_j < -\omega_j \\ -\omega_j + \dfrac{e_j+\omega_j}{\sqrt{1+(\frac{e_j+\omega_j}{\rho_j-\omega_j})^2}}, & \forall e_j > -\omega_j \end{cases} \tag{12}$$

where ω_j and ρ_j are design parameters, and both satisfy $\omega_j < \rho_j$.

Combining the backstepping technique and the virtual leader strategy, the formation controller is designed, and the generalized SC function is used to realize the anti-saturation. The ESO is applied to estimate the unmodeled dynamics, parameter perturbation and external wind wave disturbances of the unmanned vessel system. The formation controller design is as follows.

Define the position tracking error of the i-th unmanned vessel in the formation as:

$$\boldsymbol{\eta}_{ei} = \boldsymbol{\eta}_i - \boldsymbol{\eta}_{di} = \boldsymbol{\eta}_i - \boldsymbol{\eta}_t - \boldsymbol{R}(\psi_t)\boldsymbol{\varepsilon}_i \tag{13}$$

where $\boldsymbol{\varepsilon}_i$ is the relative position of each vessel and the virtual leader vessel in the formation.

According to the backstepping technique, a virtual velocity control law is designed to stabilize the position tracking error, and its expression is as follows:

$$\boldsymbol{v}_{di} = \dot{\boldsymbol{\eta}}_t - \boldsymbol{K}_i \boldsymbol{S}(\boldsymbol{\eta}_{ei}) + \dot{\boldsymbol{R}}(\psi_t)\boldsymbol{\varepsilon}_i \tag{14}$$

where $\boldsymbol{K}_i$ is a 3×3 dimensional diagonal positive definite coefficient matrix. $\mathbf{S}(\boldsymbol{\eta}_{ei}) = [s(\boldsymbol{\eta}_{ei1})\ s(\boldsymbol{\eta}_{ei2})\ s(\boldsymbol{\eta}_{ei3})]^{\mathrm{T}}$ is the designed generalized SC function, and $\boldsymbol{\eta}_{eij}$ is the j-th$(j = 1,2,3)$ element of the position tracking error $\boldsymbol{\eta}_{ei}$.

Combining Equation (13) and Equation (14), the velocity error can be defined as:

$$\boldsymbol{v}_{ei} = \dot{\boldsymbol{\eta}}_i - \boldsymbol{v}_{di} = \dot{\boldsymbol{\eta}}_{ei} + \boldsymbol{K}_i \boldsymbol{S}(\boldsymbol{\eta}_{ei}) \tag{15}$$

where $\dot{\boldsymbol{\eta}}_{ei} = \dot{\boldsymbol{\eta}}_i - \dot{\boldsymbol{\eta}}_t - \dot{\boldsymbol{R}}(\psi_t)\boldsymbol{\varepsilon}_i$.

According to Equation (3), Equation (15), and the properties (d) and (e), it can be obtained:

$$\begin{aligned} \bar{\boldsymbol{M}}_i(\boldsymbol{\eta}_i)\dot{\boldsymbol{v}}_{ei} &= \bar{\boldsymbol{M}}_i(\boldsymbol{\eta}_i)(\ddot{\boldsymbol{\eta}}_i - \dot{\boldsymbol{v}}_{di}) \\ &= \boldsymbol{R}^{-\mathrm{T}}(\psi_i)\boldsymbol{\tau}_i - \bar{\boldsymbol{C}}_i(\boldsymbol{\eta}_i, \dot{\boldsymbol{\eta}}_i)\dot{\boldsymbol{\eta}}_i - \bar{\boldsymbol{\theta}}_i(\boldsymbol{\eta}_i, \dot{\boldsymbol{\eta}}_i) - \bar{\boldsymbol{M}}_i(\boldsymbol{\eta}_i)\dot{\boldsymbol{v}}_{di} \\ &= \boldsymbol{R}^{-\mathrm{T}}(\psi_i)\boldsymbol{\tau}_i - \boldsymbol{C}_i(\boldsymbol{\eta}_i, \dot{\boldsymbol{\eta}}_i)\boldsymbol{v}_{ei} - \boldsymbol{C}_i(\boldsymbol{\eta}_i, \boldsymbol{v}_{di})\boldsymbol{v}_{ei} - \boldsymbol{C}_i(\boldsymbol{\eta}_i, \boldsymbol{v}_{di})\boldsymbol{v}_{di} - \boldsymbol{\theta}_i(\boldsymbol{\eta}_i, \dot{\boldsymbol{\eta}}_i) - \bar{\boldsymbol{M}}_i(\boldsymbol{\eta}_i)\dot{\boldsymbol{v}}_{di} \end{aligned} \tag{16}$$

where $\boldsymbol{\theta}_i(\boldsymbol{\eta}_i, \dot{\boldsymbol{\eta}}_i)$ is the compound time-varying disturbances of the system, which is an unknown three-dimensional bounded smooth function. The disturbance can be estimated according to ESO (9), and the estimated value is represented by $\hat{\boldsymbol{\theta}}_i(\boldsymbol{\eta}_i, \dot{\boldsymbol{\eta}}_i)$. Compared with neural networks which need to consider many parameters and take a long time to train the weights of the approximation strategy [40], the ESO has a simple structure, and it is much

efficient to implement, and can also improve the anti-disturbance of the entire closed-loop system.

Based on the analysis of Equations (13)–(16), combining ESO (9) and SC function (12), the formation control law of multi-unmanned vessels can be designed as:

$$\boldsymbol{\tau}_i = \boldsymbol{R}^{\mathrm{T}}(\psi_i)(\bar{\boldsymbol{C}}_i(\boldsymbol{\eta}_i, \boldsymbol{v}_{di})\boldsymbol{v}_{di} + \hat{\boldsymbol{\theta}}_i(\boldsymbol{\eta}_i, \dot{\boldsymbol{\eta}}_i) - \boldsymbol{S}(\mathrm{K}_{pi}\boldsymbol{\eta}_{ei}) - \boldsymbol{S}(\mathrm{K}_{qi}\boldsymbol{v}_{ei}) + \bar{\boldsymbol{M}}_i(\boldsymbol{\eta}_i)\dot{\boldsymbol{v}}_{di}) \tag{17}$$

where K_{pi} and K_{qi} are the adjustable positive coefficients of the controller.

3.3. System Stability Analysis

It is necessary to analyze the stability of the closed-loop feedback system composed of the ESO (9), the unmanned vessel model (3) and the controller with a SC function (17). It is assumed that parametric perturbation, external environment disturbances and internal coupling disturbances exist in the vessel system, which are all continuous bounded functions. Firstly, the following theorem is given.

Theorem 1. *For the designed closed-loop feedback system, if it meets the condition that the track points of the virtual leader vessel are smooth and bounded, and the initial system state is bounded, then the reasonable design of the controller parameters* K_{pi} *and* K_{qi} *can make all the states of the system consistent and ultimately bounded, while the position error and speed error can converge to arbitrarily small.*

Proof. Step 1. The Lyapunov function is designed as follows:

$$V = \sum_{i=1}^{n}(\sum_{j=1}^{3}\int_{\eta_{eij}(0)}^{\eta_{eij}(t)} s(\mathrm{K}_{pi}\varsigma)\mathrm{d}\varsigma + \frac{1}{2}\boldsymbol{v}_{ei}^{\mathrm{T}}\bar{\boldsymbol{M}}_i(\boldsymbol{\eta}_i)\boldsymbol{v}_{ei}) \tag{18}$$

According to the Equations (13), (15), and (16), the time derivative of V is obtained as:

$$\begin{aligned}
\dot{V} &= \sum_{i=1}^{n}(\boldsymbol{S}^{\mathrm{T}}(\mathrm{K}_{pi}\boldsymbol{\eta}_{ei})\dot{\boldsymbol{\eta}}_{ei} + \boldsymbol{v}_{ei}^{\mathrm{T}}\bar{\boldsymbol{M}}_i(\boldsymbol{\eta}_i)\dot{\boldsymbol{v}}_{ei} + \tfrac{1}{2}\boldsymbol{v}_{ei}^{\mathrm{T}}\dot{\bar{\boldsymbol{M}}}_i(\boldsymbol{\eta}_i)\boldsymbol{v}_{ei}) \\
&= \sum_{i=1}^{n}(-\boldsymbol{S}^{\mathrm{T}}(\mathrm{K}_{pi}\boldsymbol{\eta}_{ei})\boldsymbol{K}_i\boldsymbol{S}(\boldsymbol{\eta}_{ei}) + \boldsymbol{S}^{\mathrm{T}}(\mathrm{K}_{pi}\boldsymbol{\eta}_{ei})\boldsymbol{v}_{ei} + \boldsymbol{v}_{ei}^{\mathrm{T}}(\boldsymbol{R}^{-\mathrm{T}}(\psi_i)\boldsymbol{\tau}_i - \bar{\boldsymbol{C}}_i(\boldsymbol{\eta}_i, \dot{\boldsymbol{\eta}}_i)\boldsymbol{v}_{ei} - \bar{\boldsymbol{C}}_i(\boldsymbol{\eta}_i, \boldsymbol{v}_{di})\boldsymbol{v}_{ei} - \bar{\boldsymbol{C}}_i(\boldsymbol{\eta}_i, \boldsymbol{v}_{di})\boldsymbol{v}_{di} \\
&\quad -\boldsymbol{\theta}_i(\boldsymbol{\eta}_i, \dot{\boldsymbol{\eta}}_i) - \bar{\boldsymbol{M}}_i(\boldsymbol{\eta}_i)\dot{\boldsymbol{v}}_{di}) + \tfrac{1}{2}\boldsymbol{v}_{ei}{}^{\mathrm{T}}\dot{\bar{\boldsymbol{M}}}_i(\boldsymbol{\eta}_i)\boldsymbol{v}_{ei}) \\
&= \sum_{i=1}^{n}(-\boldsymbol{S}^{\mathrm{T}}(\mathrm{K}_{pi}\boldsymbol{\eta}_{ei})\boldsymbol{K}_i\boldsymbol{S}(\boldsymbol{\eta}_{ei}) + \boldsymbol{v}_{ei}^{\mathrm{T}}(-\boldsymbol{S}(\mathrm{K}_{qi}\boldsymbol{v}_{ei}) - \bar{\boldsymbol{C}}_i(\boldsymbol{\eta}_i, \boldsymbol{v}_{di})\boldsymbol{v}_{ei} - \bar{\boldsymbol{C}}_i(\boldsymbol{\eta}_i, \dot{\boldsymbol{\eta}}_i)\boldsymbol{v}_{ei} + \hat{\boldsymbol{\theta}}_i(\boldsymbol{\eta}_i, \dot{\boldsymbol{\eta}}_i) - \boldsymbol{\theta}_i(\boldsymbol{\eta}_i, \dot{\boldsymbol{\eta}}_i)) + \tfrac{1}{2}\boldsymbol{v}_{ei}{}^{\mathrm{T}}\dot{\bar{\boldsymbol{M}}}_i(\boldsymbol{\eta}_i)\boldsymbol{v}_{ei})
\end{aligned} \tag{19}$$

Step 2. Based on property (b), the following equation can be obtained:

$$-\boldsymbol{v}_{ei}^{\mathrm{T}}\bar{\boldsymbol{C}}_i(\boldsymbol{\eta}_i, \dot{\boldsymbol{\eta}}_i)\boldsymbol{v}_{ei} + \frac{1}{2}\boldsymbol{v}_{ei}^{\mathrm{T}}\dot{\bar{\boldsymbol{M}}}_i(\boldsymbol{\eta}_i)\boldsymbol{v}_{ei} = 0 \tag{20}$$

According to Equation (20), Equation (19) can be converted into the following equation:

$$\dot{V} = \sum_{i=1}^{n}(-\boldsymbol{S}^{\mathrm{T}}(\mathrm{K}_{pi}\boldsymbol{\eta}_{ei})\boldsymbol{K}_i\boldsymbol{S}(\boldsymbol{\eta}_{ei}) + \boldsymbol{v}_{ei}^{\mathrm{T}}(-\boldsymbol{S}(K_{qi}\boldsymbol{v}_{ei}) - \bar{\boldsymbol{C}}_i(\boldsymbol{\eta}_i, \boldsymbol{v}_{di})\boldsymbol{v}_{ei} + \boldsymbol{L}_i)) \tag{21}$$

where $\boldsymbol{L}_i = \hat{\boldsymbol{\theta}}_i(\boldsymbol{\eta}_i, \dot{\boldsymbol{\eta}}_i) - \boldsymbol{\theta}_i(\boldsymbol{\eta}_i, \dot{\boldsymbol{\eta}}_i)$ is the errors of the estimated disturbances.

According to the condition (6) of the Lemma 2, Equation (20) can be converted into:

$$\dot{V} \le \sum_{i=1}^{n}(-\lambda_{\min}(\boldsymbol{K}_i)\|\boldsymbol{S}(\boldsymbol{\eta}_{ei})\|^2 - \boldsymbol{v}_{ei}^{\mathrm{T}}\boldsymbol{S}(\mathrm{K}_{qi}\boldsymbol{v}_{ei}) - \|\boldsymbol{v}_{ei}\|\|\bar{\boldsymbol{C}}_i(\boldsymbol{\eta}_i, \boldsymbol{v}_{di})\boldsymbol{v}_{ei}\| + \|\boldsymbol{v}_{ei}\|\boldsymbol{L}_i) \tag{22}$$

According to the property (f), Equations (13) and (14), the following expression can be obtained:

$$\begin{aligned}\|\bar{\boldsymbol{C}}_i(\boldsymbol{\eta}_i, \boldsymbol{v}_{di})\boldsymbol{v}_{ei}\| &\leq \lambda_{\mathrm{C}i}\|\boldsymbol{v}_{di}\|\|\boldsymbol{v}_{ei}\| = \lambda_{\mathrm{C}i}\|\dot{\boldsymbol{\eta}}_{di} - \boldsymbol{K}_i\boldsymbol{S}(\boldsymbol{\eta}_{ei})\|\|\boldsymbol{v}_{ei}\| \\ &\leq \alpha_1\|\boldsymbol{v}_{ei}\| + \alpha_2\|\boldsymbol{S}(\boldsymbol{\eta}_{ei})\|\|\boldsymbol{v}_{ei}\|\end{aligned} \tag{23}$$

where $\alpha_1 > 0$ and $\alpha_2 > 0$.

By Definition 1, $\boldsymbol{v}_{ei}^{\mathrm{T}}\boldsymbol{S}(\mathrm{K}_{qi}\boldsymbol{v}_{ei}) \leq 0$. Combined with Equation (23), it can be obtained:

$$\dot{V} \leq \sum_{i=1}^{n}(-(\lambda_{\min}(\boldsymbol{K}_i) + \frac{\alpha_2}{2})\|\boldsymbol{S}(\boldsymbol{\eta}_{ei})\|^2 - (\alpha_1 + \frac{\alpha_2}{2}\|\boldsymbol{v}_{ei}\|^2)\|\boldsymbol{v}_{ei}\|^2 + \boldsymbol{E}_i) \tag{24}$$

where $\boldsymbol{E}_i = \|\boldsymbol{v}_{ei}\|\boldsymbol{L}_i$. Choose the appropriate parameters α_1 and α_2, it can be obtained that $\alpha_{\mathrm{m}} = \alpha_1 + \frac{\alpha_2}{2}\|\boldsymbol{v}_{ei}\|^2 > 0$.

According to the conditions (1) and (5) of the Lemma 2, Equation (24) can be obtained as follows:

$$\dot{V} \leq \sum_{i=1}^{n}(-(\lambda_{\min}(\boldsymbol{K}_i) + \frac{\alpha_2}{2})s'^2_{\mathrm{M}}\|\boldsymbol{\eta}_{ei}\|^2 - \alpha_m\|\boldsymbol{v}_{ei}\|^2 + \boldsymbol{E}_i) \tag{25}$$

Step 3: According to the conditions (2)–(4) of the Lemma 2, it gives $V > 0$, and obtains:

$$V \leq \sum_{i=1}^{n}(\frac{\mathrm{K}_{pi}s'_{\mathrm{M}}}{2}\|\boldsymbol{\eta}_{ei}\|^2 + \frac{\lambda_{\max}(\bar{\boldsymbol{M}}_i)}{2}\|\boldsymbol{v}_{ei}\|^2) \tag{26}$$

According to Equations (25) and (26), it can be obtained:

$$\dot{V} \leq -2\mu V + \boldsymbol{E} \tag{27}$$

where $\boldsymbol{E} = \sum_{i=1}^{n}\boldsymbol{E}_i$, $\mu = \min\left\{\frac{(\lambda_{\min}(\boldsymbol{K}_i)+\frac{\alpha_2}{2})s'_{\mathrm{M}}}{\mathrm{K}_{pi}}, \frac{\alpha_m}{\lambda_{\max}(\bar{\boldsymbol{M}}_i)}\right\}$.

According to the above analysis, it gives:

$$V \leq \frac{\boldsymbol{E}}{2\mu} + (V(0) - \frac{\boldsymbol{E}}{2\mu})e^{-2\mu t} \tag{28}$$

According to Lemma 1, $\lim_{t\to\infty}\boldsymbol{E} < \sigma$ can be obtained, where σ is an arbitrarily small three-dimensional positive vector. Therefore, all states are consistent and ultimately bounded in the closed-loop system. When $t \to \infty$, $V \leq \frac{\boldsymbol{E}}{2\mu}$, and it can be obtained:

$$\lim_{t\to\infty}\|\boldsymbol{\eta}_{ei}\| \leq \sqrt{\frac{\boldsymbol{E}_i}{\mu\mathrm{K}_{pi}s'_{\mathrm{M}}}} \tag{29}$$

$$\lim_{t\to\infty}\|\boldsymbol{v}_{ei}\| \leq \sqrt{\frac{\boldsymbol{E}_i}{\mu\lambda_{\max}(\bar{\boldsymbol{M}}_i)}} \tag{30}$$

The position error and velocity error can be arbitrarily small by choosing appropriate parameters. The proof is complete. □

4. Simulation Results and Analysis

In order to verify the effectiveness, anti-disturbance, and anti-saturation of the proposed formation controller in the presence of model uncertainty, parameter perturbation and unknown environmental disturbances, the vessel model with a length of 1.2 m is

selected for simulation analysis. The parameter values of unmanned vessels are shown in Table 1 [41].

Table 1. Model parameter values of unmanned vessels in formation.

Parameter	Value	Parameter	Value
m_{11i}	25.8 (kg)	d_{11i}	0.72 (kg × m/s)
m_{22i}	33.8 (kg)	d_{22i}	0.8896 (kg × m/s)
m_{33i}	2.76 (kg)	d_{33i}	1.9 (kg × m/s)
m_{23i}	1.0115 (kg)	d_{23i}	7.25 (kg × m/s)
m_{32i}	1.0115 (kg)	d_{32i}	0.0313 (kg × m/s)

An experiment with three unmanned vessels applied to verify the effectiveness and applicability of the formation controller. The initial conditions of unmanned vessels in the simulation are as follows:

The initial position and heading angle of the virtual leader vessel is set as:

$$\boldsymbol{\eta}_t = [0\ 50\ 0^\circ]^{\mathrm{T}} \tag{31}$$

The initial position and heading angle of the three follower vessels are set as:

$$\boldsymbol{\eta}_1 = [-10\ 46\ 1^\circ]^{\mathrm{T}}, \boldsymbol{\eta}_2 = [-15\ 40\ 1^\circ]^{\mathrm{T}}, \boldsymbol{\eta}_3 = [-20\ 60\ 1^\circ]^{\mathrm{T}} \tag{32}$$

The initial velocity of both the follower vessel and the virtual leader vessel are set to:

$$\boldsymbol{v} = [0\ 0\ 0]^{\mathrm{T}} \tag{33}$$

The relative positions of three follower vessels and virtual leader vessel are respectively set as follows:

$$\boldsymbol{\varepsilon}_1 = [0\ 0\ 0^\circ]^{\mathrm{T}}, \boldsymbol{\varepsilon}_2 = [0\ -5\ 0^\circ]^{\mathrm{T}}, \boldsymbol{\varepsilon}_3 = [0\ 5\ 0^\circ]^{\mathrm{T}} \tag{34}$$

The trajectory of virtual leader vessel is set as:

$$\begin{cases} y_d = 50, & 0 \le t < 40\pi \\ \mathrm{y}_d = 30 + 20\cos(0.05t), & 40\pi \le t < 60\pi \\ \mathrm{y}_d = 10, & 60\pi \le t < 100\pi \end{cases} \quad \begin{cases} x_d = t, & 0 \le t < 40\pi \\ x_d = 40\pi + 20\sin(0.05t), & 40\pi \le t < 60\pi \\ x_d = 100\pi - t, & 60\pi \le t < 100\pi \end{cases} \tag{35}$$

It is a 'U' trajectory composed of double straight lines and a semicircle, including the conversion between the straight lines and the semicircle. The unmanned vessel relies on the effective control law of the controller to track the expected trajectory during the conversion process. Therefore, the 'U' trajectory can be used to verify the effectiveness of the controller. The heading angle of the virtual leader vessel is calculated by $\psi_d = \arctan(\dot{y}_d/\dot{x}_d)$.

Assuming that the coefficients m_{11i}, m_{22i}, m_{33i}, m_{23i}, m_{32i}, d_{11i}, d_{22i}, d_{33i}, d_{23i} and d_{32i} of each vessel have an error of 5%. The model uncertainty and internal disturbances $\boldsymbol{\tau}_{gi}$ and the external disturbances $\boldsymbol{\tau}_{di}$ of the three vessels can be set as follows:

$$\boldsymbol{\tau}_{gi} = [v_i^3 + 0.01u_i\ u_i r_i + 0.02u_i u_i r_i + 0.2r_i^2]^{\mathrm{T}} \tag{36}$$

$$\boldsymbol{\tau}_{di} = \begin{bmatrix} v_i^3 + 0.51u_i + 0.09\cos(0.5t) + 0.06\sin(0.5t) \\ u_i r_i + 0.62u_i + 0.09\sin(0.5t) \\ 0.4u_i r_i + 0.15v_i^2 + 0.04\sin(0.5t) \end{bmatrix} \tag{37}$$

In order to accurately describe the error between the compound disturbances suffered by unmanned vessel and its estimated value, the compound disturbances suffered by

each vessel is expressed as $\|\boldsymbol{\theta}_i\|$, where $\boldsymbol{\theta}_i = [\tau_{du}\ \tau_{dv}\ \tau_{dr}]^{\mathrm{T}}$. Similarly, the total velocity error of the unmanned vessel is denoted by $\|\boldsymbol{v}_{ei}\|$. In practical engineering, because of the physical constraints of the actuator of vessel, the control force and torque can be expressed as follows:

$$\boldsymbol{\tau}_i = \begin{cases} \boldsymbol{\tau}_{\min}, \boldsymbol{\tau}_i \leq \boldsymbol{\tau}_{i\min} \\ \boldsymbol{\tau}_i, \boldsymbol{\tau}_{i\min} < \boldsymbol{\tau}_i < \boldsymbol{\tau}_{i\max} \\ \boldsymbol{\tau}_{i\max}, \boldsymbol{\tau}_i \geq \boldsymbol{\tau}_{i\max} \end{cases} \tag{38}$$

The input saturation limits of follower vessels are shown in Table 2.

Table 2. Input saturation limits.

Parameter	Value	Parameter	Value
$\tau_{ui\min}$	−9.2 (N)	$\tau_{ui\max}$	9.2 (N)
$\tau_{vi\min}$	−4.5 (N)	$\tau_{vi\max}$	4.5 (N)
$\tau_{ri\min}$	−3.0 (N)	$\tau_{ri\max}$	3.0 (N)

According to the saturation values of force and torque, the parameters of the SC function are selected as:

$$\omega_j = 0.59, \rho_j = 0.6 \tag{39}$$

The parameters of ESO are selected as follows:

$$\lambda_1 = 0.9, \lambda_2 = 3, \lambda_3 = 8.9, \beta = 0.5, \delta_1 = \delta_2 = \delta_3 = 0.1 \tag{40}$$

The parameters of the formation controller are selected as follows:

$$\mathrm{K}_{pi} = 10, \mathrm{K}_{qi} = 10, \boldsymbol{K}_i = diag(0.65\ 1\ 1.2) \tag{41}$$

The high gain observer (HGO) can estimate the derivative term of the system output according to the output of the system [42] and does not depend on the mathematical model of the system, and is widely used in nonlinear output feedback control. This is similar to the role of ESO. According to Equation (7), the designed dynamic equation of HGO is as follows [43]:

$$\dot{\hat{\boldsymbol{d}}}(t) = -\mathrm{Y}\hat{\boldsymbol{d}}(t) + \mathrm{Y}\boldsymbol{d}(t) \tag{42}$$

where $\boldsymbol{d}(t) = \boldsymbol{\theta}_i(\boldsymbol{\eta}_i, \dot{\boldsymbol{\eta}}_i)$ is the compound disturbance. $\hat{\boldsymbol{d}}(t)$ is the estimated value of $\boldsymbol{d}(t)$, Y is the observer gain coefficient. The Laplace transform of Equation (40) is as follows:

$$\hat{\boldsymbol{D}}(s) = \frac{\mathrm{Y}}{s + \mathrm{Y}}\boldsymbol{D}(s) \tag{43}$$

where $\hat{\boldsymbol{D}}(s)$ and $\boldsymbol{D}(s)$ are the Laplace transform of $\hat{\boldsymbol{d}}(t)$ and $\boldsymbol{d}(t)$ respectively. It can get $\hat{\boldsymbol{D}}(s) \approx \boldsymbol{D}(s)$ by selecting the appropriate parameter Y, i.e., $\hat{\boldsymbol{d}}(t) \approx \boldsymbol{d}(t)$.

Therefore, this simulation experiment compares the designed SC-ESO scheme with HGO scheme and ESO scheme respectively, which can effectively verify the performance of the designed SC-ESO scheme. The simulation time is set as 100π seconds. The simulation results and corresponding analysis are described as follows. Formation trajectories of virtual leader vessel and three unmanned vessels based on SC-ESO and backstepping are shown in Figure 4.

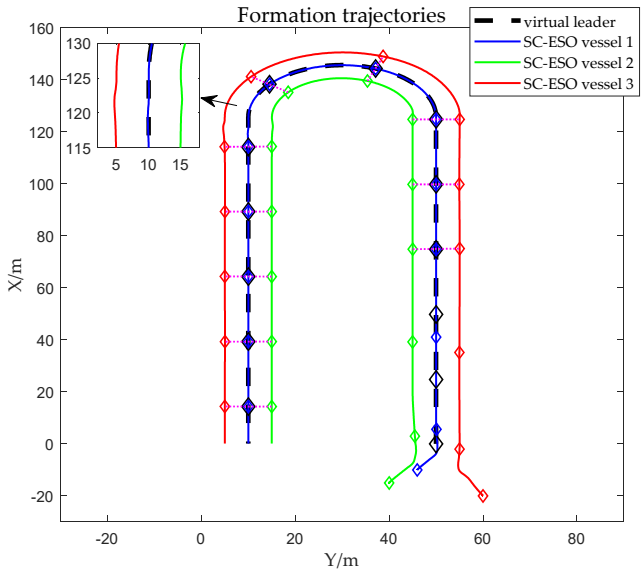

Figure 4. Formation trajectories of virtual leader vessel and three unmanned vessels based on SC-ESO and backstepping. (The rhombus indicates the unmanned vessel).

As shown in Figure 4, the pink dotted line represents the formation shape of three unmanned vessels, the black dash line represents the trajectory of the virtual leader vessel, the initial position of three follower vessels are $[x_1, y_1] = [-10, 46]$, $[x_2, y_2] = [-15, 40]$, and $[x_3, y_3] = [-20, 60]$, and the proposed SC-ESO represents the combination of saturated constraint function and extended state observer. It can be seen From Figure 4, that the vessels in the formation can track the desired track in a relatively short period of time and maintain the same formation as the virtual vessel, when the initial position error of the vessel is large. The unmanned vessel using the proposed SC-ESO can track their formation in about 75 s. The position of the vessel is sampled every 25 s, that is, at the time of the third sampling, the formation trajectory can be tracked, as shown in the pink dotted line in Figure 4. When the tracking trajectory changes from a straight line to a semicircular trajectory, the trajectories of the three unmanned vessels will fluctuate, but the desired trajectory can be tracked in a short time. Therefore, the 'U' trajectory can validly verify the effectiveness and applicability of the controller proposed in this paper. The comparison of the backstepping control method using SC-ESO, ESO, HGO and without observer is shown in Figure 5.

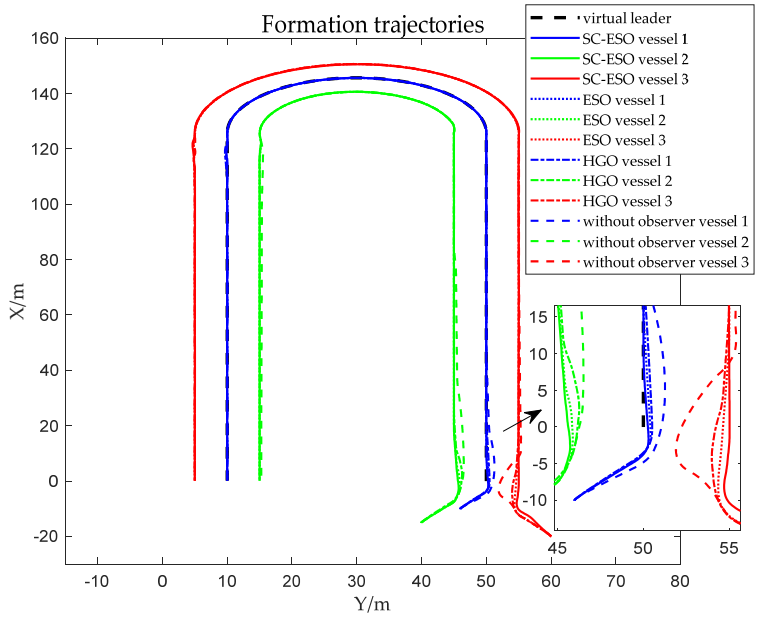

Figure 5. Comparison results with SC-ESO, ESO, HGO and without observer.

In Figure 5, the solid line indicates the case with SC-ESO, the dotted line for the case with ESO, the dash-dot line for the case HGO, and the dash line indicates the case without observer. From Figure 5, it shows that the trajectory tracking effect of the proposed SC-ESO scheme are better than ESO scheme and HGO scheme, which demonstrates that the effectiveness and superiority of the proposed SC-ESO. The control method without observer and saturation constraint is easy to cause collisions between unmanned vessels and destroy formation because of the distance between unmanned vessels is too close. It can be seen from the results that the proposed SC-ESO scheme can improve the control performance of the system under model uncertainties, parameter perturbation and external disturbances. The position error between each unmanned vessel and its desired trajectory is shown in Figures 6 and 7.

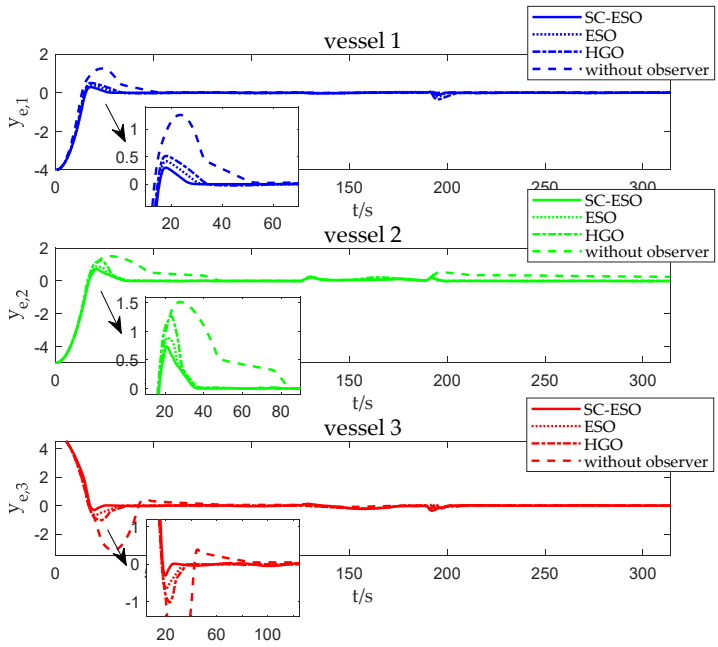

Figure 6. The position error between each unmanned vessel and its desired trajectory in the Y direction.

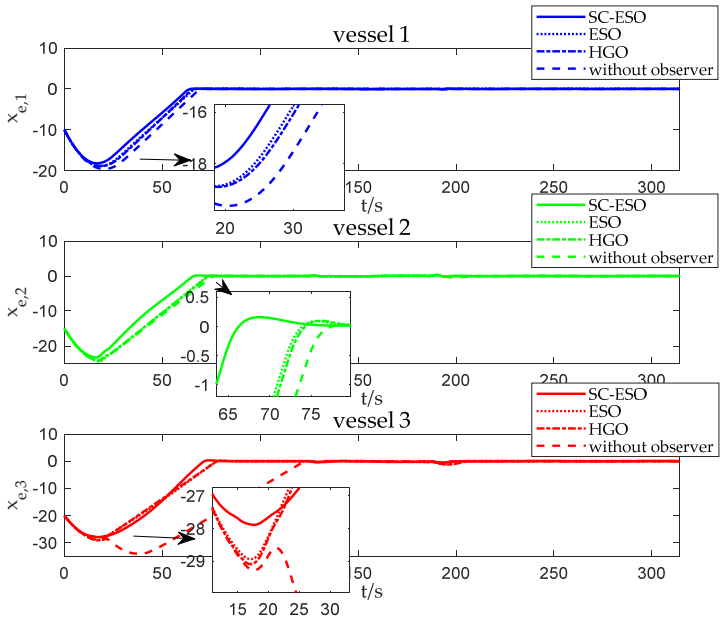

Figure 7. The position error between each unmanned vessel and its desired trajectory in the X direction.

In Figures 6 and 7, the solid line indicates the case with SC-ESO, the dotted line for the case with ESO, the dash-dot line for the case HGO and the dash line indicates the case without ESO. Where $y_{e,i}$ is the position error of the i-th vessel in the Y direction, and $x_{e,i}$ is the position error of the i-th vessel in the X direction. It can be seen that the initial position of each unmanned vessel is far away from its desired trajectory, and the initial position error is large, but they can track the desired trajectory eventually. Moreover, under the action of the controller (17) proposed in this paper, the control system convergence rate of tracking error is better than the HGO scheme and the ESO scheme, and the overshoot is also the smallest, which proves the effectiveness of the SC-ESO controller proposed in this paper. Therefore, in order to improve the control accuracy, SC-ESO is required. The total velocity errors of each unmanned vessel are shown in Figure 8.

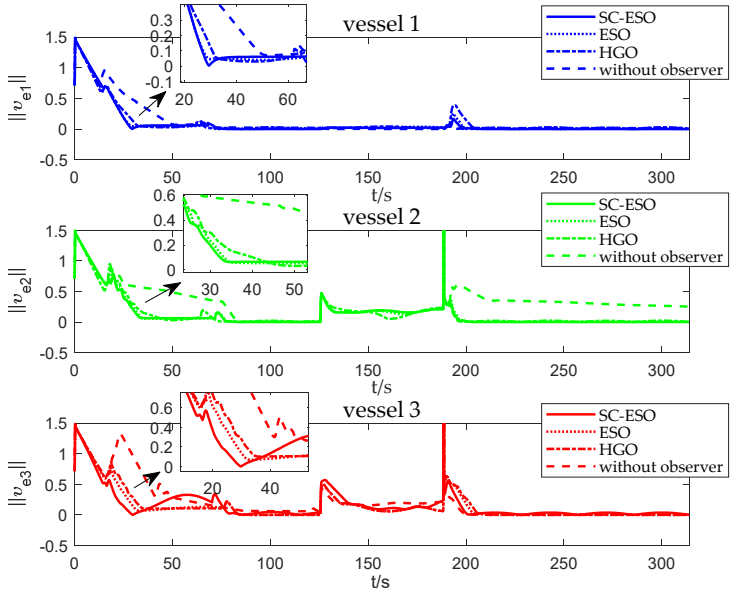

Figure 8. The total velocity error of unmanned vessel.

It can be seen from Figure 8 that the velocity error of the unmanned vessel system using the SC-ESO converges faster compared with other cases, which demonstrates that

the SC-ESO scheme enables the unmanned vessels to form formations faster. The velocity errors will fluctuate when the straight track and the semicircle track are converted, and the unmanned vessels formation can maintain the same velocity after a period of adjustment. Under the action of the controller (17), the position error and velocity error converge to an arbitrarily small range, which proves that the proposed control scheme guarantees that all signals in the closed-loop control system are uniformly converges to near zero and tracking error can be adjusted by a predefined parameter. Moreover, the comprehensive performance comparison of the position and velocity tracking errors of the three unmanned vessels in the formation are shown in Table 3.

Table 3. Comparison of position and speed error performance of the four schemes.

Tracking Error	Calculational Method	SC-ESO	ESO	HGO	Without Observer
$y_{e,1}$	IAE	43.5229	46.8453	51.0188	62.3349
	RMSE	5.8023	6.2423	6.7945	8.2916
$y_{e,2}$	IAE	68.7059	71.9392	77.3223	149.6374
	RMSE	9.1452	9.5730	10.2854	19.8503
$y_{e,3}$	IAE	70.3077	72.5880	74.1627	123.3579
	RMSE	9.3580	9.6589	9.8679	16.3768
$x_{e,1}$	IAE	724.6610	788.2075	789.1343	864.3512
	RMSE	95.9790	104.3932	104.5158	114.4674
$x_{e,2}$	IAE	905.6605	1071.9	1072.9	1105.4
	RMSE	119.9877	141.9806	142.1105	146.4097
$x_{e,3}$	IAE	1356.0	1375.1	1385.9	2624.7
	RMSE	179.6202	182.1530	183.5760	347.4835
$\|\boldsymbol{v}_{e1}\|$	IAE	25.3042	26.5956	30.2307	36.2265
	RMSE	3.3568	3.5276	4.0084	4.8015
$\|\boldsymbol{v}_{e2}\|$	IAE	55.9452	56.5582	58.0371	118.0017
	RMSE	7.9342	8.0152	8.2104	16.1418
$\|\boldsymbol{v}_{e3}\|$	IAE	61.5521	59.3313	64.5834	80.7873
	RMSE	8.6783	8.3844	9.0763	11.2202

The integral time square error (IAE), i.e., IAE $= \int_0^t |e(\varsigma)| \mathrm{d}\varsigma$, the root-mean-square error (RMSE), i.e., RMSE $= (\frac{1}{t}\int_0^t e^2(\varsigma)\mathrm{d}\varsigma)^{1/2}$, are utilized to assess the tracking effect and steady state performance in trajectory tracking of unmanned vessel. The smaller the values of IAE and RESM, the better the control effect of the scheme used. According to the comparative analysis of the data in Table 3, the tracking effect and steady state performance of the formation controller based on SC-ESO are significantly better than other schemes. The control effect of the ESO scheme and HGO scheme are slightly worse than the proposed SC-ESO. The scheme without observer has the worst effect. The surge force, sway force, and yaw torque of three unmanned vessels are shown in Figures 9 and 10.

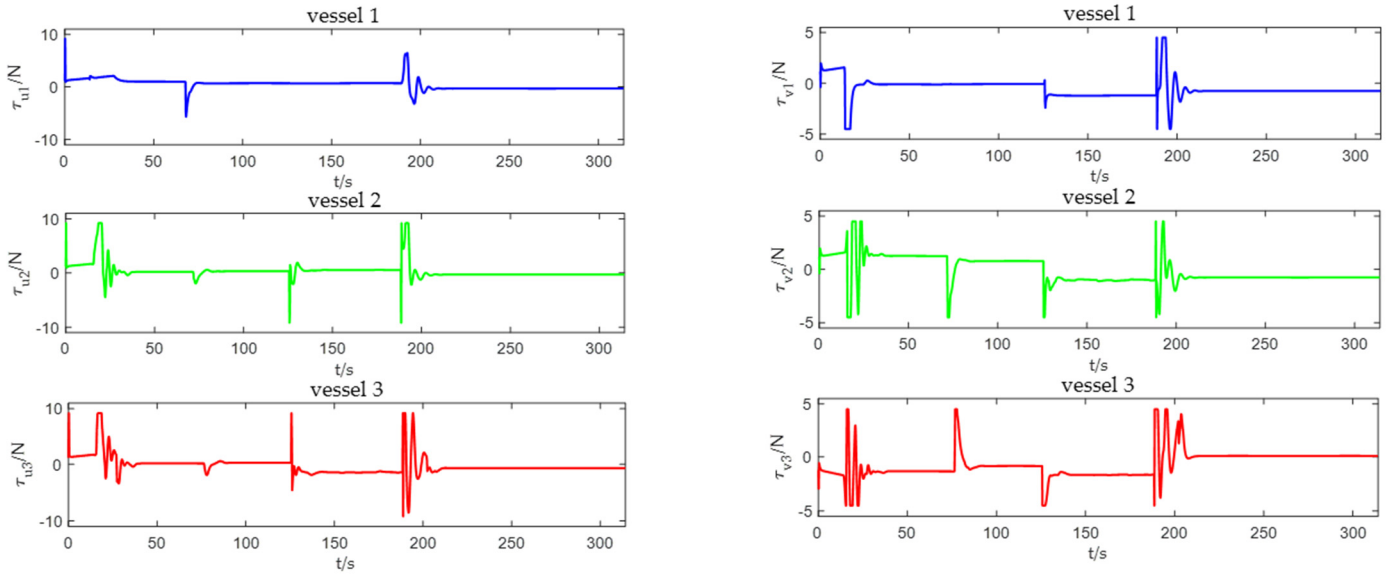

Figure 9. The surge force and sway force of three unmanned vessels.

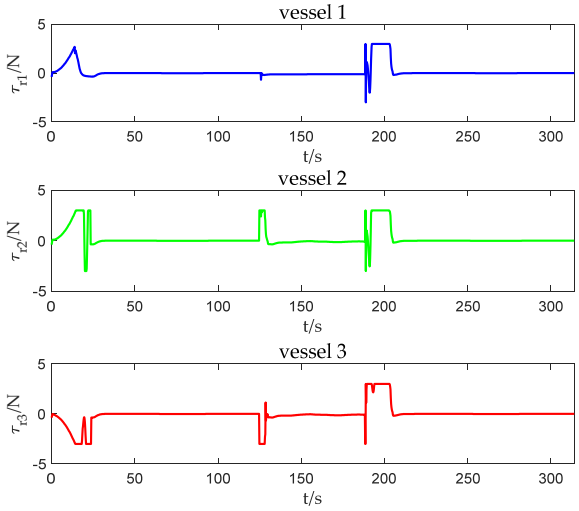

Figure 10. The yaw torque of three unmanned vessels.

As shown in Figures 9 and 10, in order to track the desired trajectory, the force and torque of the unmanned vessel fluctuate dramatically in about 15 to 30 s. When the desired trajectory transforms from the straight path to the semicircle path and from the semicircle path to the straight path, both force and torque fluctuate in about 120 to 130 s and 190 to 220 s, respectively. Under the limitation of input saturation value, it can be seen from Figures 9 and 10 that the surge force τ_{ui}, sway force τ_{vi}, and yaw torque τ_{ri} do not exceed the actuator saturation values showed in Table 2, which fully indicates the anti-saturation performance of the controller with the proposed SC function, and it is much suitable for engineering application. The disturbances estimation results of the three unmanned vessels by ESO are shown in Figures 11–14.

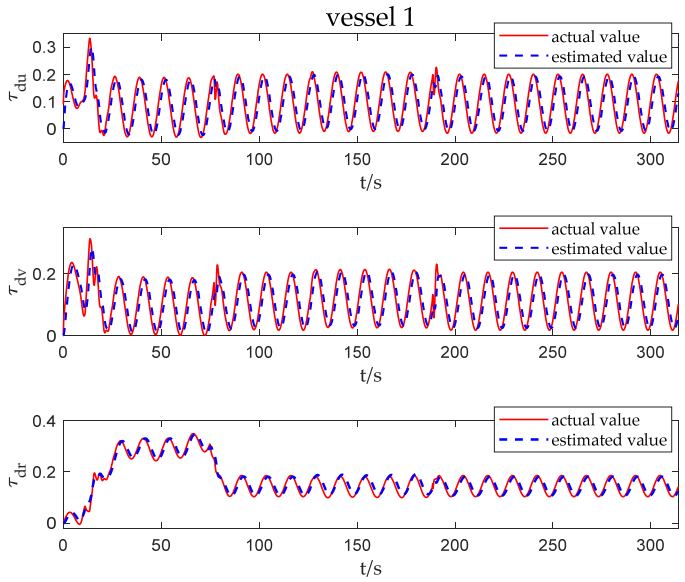

Figure 11. The disturbances estimation of vessel 1 by ESO in surge, sway, and yaw directions.

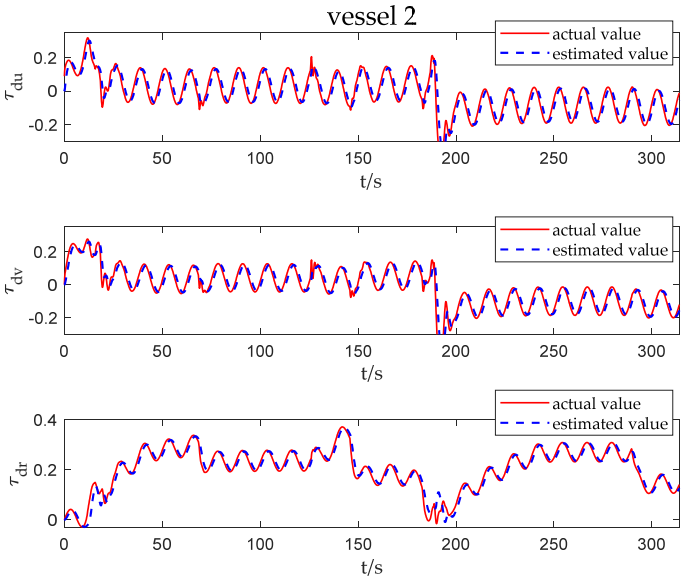

Figure 12. The disturbances estimation of vessel 2 by ESO in surge, sway, and yaw directions.

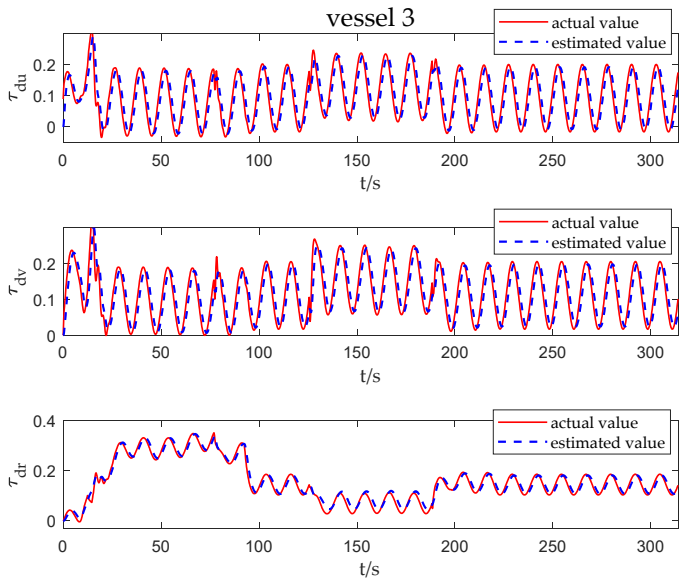

Figure 13. The disturbances estimation of vessel 3 by ESO in surge, sway, and yaw directions.

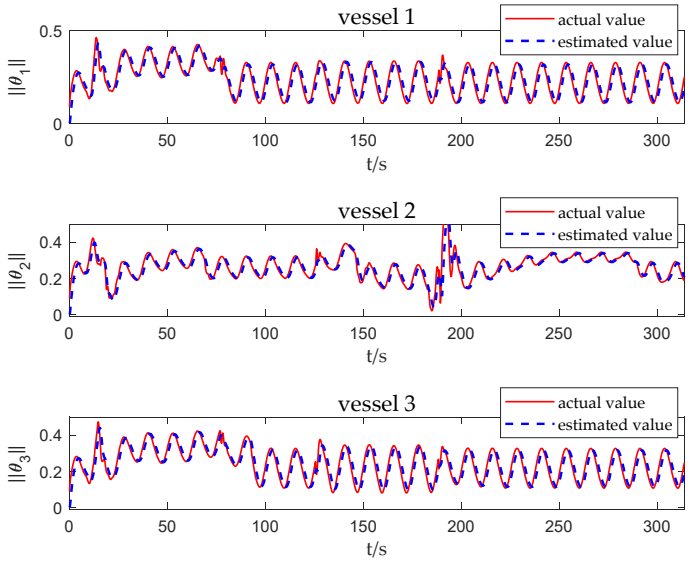

Figure 14. The compound disturbances estimation of three unmanned vessels by ESO.

Figures 11–13 show the estimation of the disturbances from three unmanned vessels in the direction of surge, sway, and yaw by ESO, which includes internal unmodeled dynamics, parameter perturbation, and unknown environmental disturbances. Figure 14 shows the estimated compound disturbances of three unmanned vessels by ESO. The red solid line represents the actual disturbances of three unmanned vessels, and the blue dash line represents the estimate of the actual disturbances using ESO. The results show that ESO can estimate disturbances well. The better the estimation effect is, the stronger the anti-disturbance performance of the controller and the higher the control accuracy. The estimation errors of compound disturbances by ESO are shown in Figure 15.

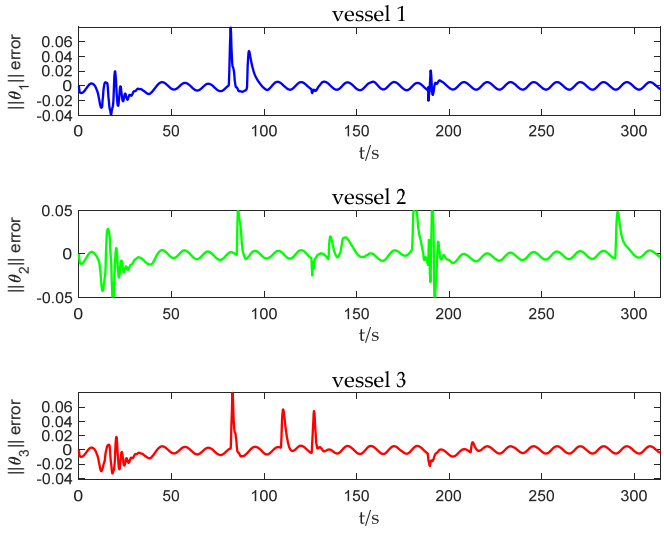

Figure 15. The estimation errors by ESO of three vessels.

Figure 15 shows the variation of the error between the estimated value obtained using ESO and the actual compound disturbances value of the three unmanned vessels. It can be seen that most of the estimation error does not exceed 0.02. According to the simulation results, the ESO has a good estimation effect on the compound disturbances of vessel. From the above comparison results, it follows that the proposed SC-ESO and backstepping scheme is more effective for the formation control system with model uncertainties, parameter perturbation, and external environmental disturbances.

5. Conclusions

In this paper, a formation control method based on ESO for unmanned surface vessels with control forces saturation constraint was proposed. First, considering the presence of model uncertainty, parameter perturbation, and unknown environmental disturbances, the ESO was designed to estimate the internal and external compound disturbances of the unmanned vessel. Using the virtual leader formation control strategy, combined with the backstepping and SC function, an anti-saturation formation controller was proposed for unmanned vessels based on ESO. Then, it was proven that the designed ESO can make the error between the estimated value and the real value converged to an arbitrary small by choosing reasonable parameters. The stability of the closed-loop system was analyzed with Lyapunov method, and it was proved that the whole system was uniform and eventually bounded. Finally, through the comparative analysis of simulation experiments, the control method based on SC-ESO and backstepping was converged and effective in the presence of the compound disturbances, which could precisely realize the anti-saturation formation control of multi-unmanned vessels.

Author Contributions: Conceptualization, H.F. and Y.W.; methodology, H.F., S.W. and Y.W.; software, S.W.; validation S.W. and Y.W.; writing—original draft preparation, S.W.; writing—review and editing, H.F., S.W. and Y.J. All authors have read and agreed to the published version of the manuscript.

Funding: This research was funded by National Natural Science Foundation of China, grant number 52071112; Fundamental Research Funds for the Central Universities, grant number 3072021CFJ0408.

Institutional Review Board Statement: Not applicable.

Informed Consent Statement: Not applicable.

Data Availability Statement: Not applicable.

Conflicts of Interest: The authors declare no conflict of interest. The funders had no role in the design of the study.

References

1. Li, Y.Z.; Wu, Y.Q.; He, S.H. Network-based leader-following formation control of second-order autonomous unmanned systems. *J. Frankl. Inst.* **2021**, *358*, 757–775. [CrossRef]
2. Ren, H.; Karimi, H.R.; Lu, R.; Wu, Y. Synchronization of network systems via aperiodic sampled-data control with constant delay and application to unmanned ground vehicles. *IEEE Trans. Ind. Electron.* **2020**, *67*, 4980–4990. [CrossRef]
3. Cho, G.R.; Li, J.H.; Park, D.; Jung, J.H. Robust trajectory tracking of autonomous underwater vehicles using back-stepping control and time delay estimation. *Ocean Eng.* **2020**, *201*, 107131. [CrossRef]
4. Lu, Q.; Li, Z.; Yu, L.; Su, C.Y. Adaptive visual regulation of wheeled mobile robots: A switching approach. *J. Intell. Robot. Syst.* **2020**, *98*, 345–358. [CrossRef]
5. Riahifard, A.; Rostami, S.M.H.; Wang, J.; Kim, H.J. Adaptive Leader-Follower Formation Control of under-Actuated Surface Vessels with Model Uncertainties and Input Constraints. *Appl. Sci.* **2019**, *9*, 3901. [CrossRef]
6. Ren, J.; Song, Q.; Gao, Y.; Lu, G. Leader-following bipartite consensus of second-order time-delay nonlinear multi-agent systems with event-triggered pinning control under signed digraph. *Neurocomputing* **2020**, *385*, 186–196. [CrossRef]
7. Liu, Z.W.; Zhou, H.; Wang, Y.W. Formation-containment control of multiple underactuated surface vessels with sampling communication via hierarchical sliding mode approach. *ISA Trans.* **2019**, *12*, 1–10. [CrossRef]
8. Park, B.S.; Yoo, S.J. Connectivity-maintaining and collision-avoiding performance function approach for robust leader–follower formation control of multiple uncertain underactuated surface vessels. *Automatica* **2021**, *127*, 1–10. [CrossRef]
9. Shojaei, K. Observer-based neural adaptive formation control of autonomous surface vessels with limited torque. *Robot. Auton. Syst.* **2016**, *78*, 83–96. [CrossRef]
10. Oh, S.R.; Sun, J. Path following of underactuated marine surface vessels using line-of-sight based model predictive control. *Ocean Eng.* **2010**, *37*, 289–295. [CrossRef]
11. Ghommam, J.; Mnif, F.; Benali, A.; Derbel, N. Asymptotic backstepping stabilization of an underactuated surface vessel. *IEEE Trans. Control Syst. Technol.* **2006**, *14*, 1150–1157. [CrossRef]
12. Ghommam, J.; Mnif, F. Coordinated path-following control for a group of underactuated surface vessels. *IEEE Trans. Ind. Electron.* **2009**, *56*, 3951–3963. [CrossRef]
13. Xu, J.; Wang, M.; Qiao, L. Dynamical sliding mode control for the trajectory tracking of underactuated unmanned underwater vehicles. *Ocean Eng.* **2015**, *105*, 54–63. [CrossRef]
14. Sun, Z.; Zhang, G.; Lu, Y. Leader-Follower Formation Control of Underactuated Surface Vehicles based on Sliding Mode Control and Parameter Estimation. *ISA Trans.* **2018**, *72*, 15–24. [CrossRef]
15. Skjetne, R.; Moi, S.; Fossen, T.I. Nonlinear Formation Control of Marine Craft. In Proceedings of the 41st IEEE Conference on Decision and Control, Las Vegas, NV, USA, 10–13 December 2002; pp. 1699–1704.
16. Beard, R.W.; Lawton, J.; Hadaegh, F.Y. A coordination architecture for spacecraft formation control. *IEEE Trans. Control Syst. Technol.* **2001**, *9*, 777–790. [CrossRef]
17. Cui, R.; Ge, S.S.; How, B.V.E.; Choo, Y.S. Leader–follower formation control of underactuated autonomous underwater vehicles. *Ocean Eng.* **2010**, *37*, 1491–1502. [CrossRef]
18. Ghommam, J.; Saad, M. Adaptive Leader–Follower Formation Control of Underactuated Surface Vessels Under Asymmetric Range and Bearing Constraints. *IEEE Trans. Veh. Technol.* **2018**, *67*, 852–865. [CrossRef]
19. Ren, W.; Beard, R.W. Formation feedback control for multiple spacecraft via virtual structures. *IEEE Proc. Control Theory Appl.* **2004**, *151*, 357–368. [CrossRef]
20. Fu, M.; Jiao, J. Passive coordinated formation control for vessels based on virtual leader. *Acta Autom. Sin.* **2014**, *40*, 439–448.
21. Kim, E.; Fan, S.; Bose, N.; Nguyen, H. Current Estimation and Path Following for an Autonomous Underwater Vehicle (AUV) by Using a High-gain Observer Based on an AUV Dynamic Model. *Int. J. Control Autom. Syst.* **2020**, *19*, 478–490. [CrossRef]
22. Jin, X. Fault tolerant finite-time leader-follower formation control for autonomous surface vessels with LOS range and angle constraints. *Automatica* **2016**, *68*, 228–236. [CrossRef]
23. Yu, J.; Dong, X.; Li, Q.; Ren, Z. Practical time-varying formation tracking for second-order nonlinear multiagent systems with multiple leaders using adaptive neural networks. *IEEE Trans. Neural Netw. Learn. Syst.* **2018**, *29*, 6015–6025. [CrossRef]
24. Wang, J.; Wang, C.; Wei, Y. Neuroadaptive Sliding Mode Formation Control of Autonomous Underwater Vehicles with Uncertain Dynamics. *IEEE Syst. J.* **2019**, *14*, 3325–3333. [CrossRef]
25. Peng, Z.; Wang, D.; Chen, Z.; Hu, X.; Lan, W. Adaptive dynamic surface control for formations of autonomous surface vehicles with uncertain dynamics. *IEEE Trans. Control Syst. Technol.* **2013**, *21*, 513–520. [CrossRef]
26. Shojaei, K.; Dolatshahi, M. Line-of-sight target tracking control of underactuated autonomous underwater vehicles. *Ocean Eng.* **2017**, *133*, 244–252. [CrossRef]
27. Liu, S.; Liu, Y.; Wang, N. Nonlinear disturbance observer-based backstepping finite-time sliding mode tracking control of underwater vehicles with system uncertainties and external disturbances. *Nonlinear Dyn.* **2017**, *88*, 465–476. [CrossRef]
28. Peng, Z.; Wang, J. Output-Feedback Path-Following Control of Autonomous Underwater Vehicles Based on an Extended State Observer and Projection Neural Networks. *IEEE Trans. Syst.* **2018**, *48*, 535–544. [CrossRef]
29. Wei, H.; Zhao, Y. Adaptive Neural Network Control of a Marine Vessel with Constraints Using the Asymmetric Barrier Lyapunov Function. *IEEE Trans. Cybern.* **2017**, *47*, 1641–1651.
30. Lin, A.; Jiang, D.; Zeng, J. Underactuated Vessel Formation Control with Input Saturation. *Acta Autom. Sin.* **2018**, *44*, 1496–1504.

31. Li, L.; Dong, K.; Guo, G. Trajectory tracking control of underactuated surface vessel with full state constraints. *Asian J. Control.* **2020**, 1–10. [CrossRef]
32. Shojaei, K. Neural network formation control of underactuated autonomous underwater vehicles with saturating actuators. *Neurocomputing* **2016**, *194*, 372–384. [CrossRef]
33. Zheng, Z.; Huang, Y.; Xie, L.; Zhu, B. Adaptive Trajectory Tracking Control of a Fully Actuated Surface Vessel with Asymmetrically Constrained Input and Output. *IEEE Trans. Control Syst. Technol.* **2018**, *26*, 1851–1859. [CrossRef]
34. Yu, C.; Xiang, X.; Wilson, P.A.; Zhang, Q. Guidance-Error-Based Robust Fuzzy Adaptive Control for Bottom Following of a Flight-Style AUV with Saturated Actuator Dynamics. *IEEE Trans. Cybern.* **2020**, *50*, 1887–1899. [CrossRef] [PubMed]
35. Shojaei, K. Leader–follower formation control of underactuated autonomous marine surface vehicles with limited torque. *Ocean Eng.* **2015**, *105*, 196–205. [CrossRef]
36. Fossen, T.I. *Handbook of Marine Craft Hydrodynamics and Motion Control*, 1st ed.; John Wiley & Sons Ltd.: Hoboken, NJ, USA, 2011; pp. 83–126.
37. Breivik, M.; Hovstein, V.E.; Fossen, T.I. Vessel formation control: A guided leader-follower approach. In Proceedings of the 17th IFAC World Congress, Seoul, South Korea, 6–11 July 2008; pp. 16008–16014.
38. Huang, Y.; Han, J.G. A new synthesis method for uncertain systems the Self-Stable Region approach. *Int. J. Syst. Sci.* **1999**, *30*, 33–38. [CrossRef]
39. Aguinaga, R.E.; Zavala, R.A.; Santibanez, V.; Reyes, F. Global Trajectory Tracking Through Static Feedback for Robot Manipulators with Bounded Inputs. *IEEE Trans. Control Syst. Technol.* **2009**, *17*, 934–944. [CrossRef]
40. Li, T.S.; Feng, G.; Wang, D.; Tong, S.C. Neural-network-based simple adaptive control of uncertain multi-input multi-output non-linear systems. *IET Control Theory Appl.* **2010**, *4*, 1543–1557. [CrossRef]
41. Skjetne, R.; Fossen, T.I.; Kokotovic, P.V. Adaptive maneuvering, with experiments, for a model vessel in a marine control laboratory. *Automatica* **2005**, *41*, 289–298. [CrossRef]
42. GE, S.S.; Zhang, J. Neural-network control of nonaffine nonlinear system with zero dynamics by state and output feedback. *IEEE Trans. Neural Netw.* **2003**, *14*, 900–918.
43. Freidovich, L.B.; Kahlil, H.K. Performance recovery of feedback-linearization-based designs. *IEEE Trans. Autom. Control* **2008**, *53*, 2324–2334. [CrossRef]